# The Motion and Boundary Between the Capricorn and Australian Plates

Jean-Yves Royer and Richard G. Gordon

**The motions between the Somalian, Antarctic, and Australian plates—the three plates believed to meet at the Rodrigues triple junction in the Indian Ocean—are inconsistent with the assumption that all three plates are rigid. The discrepancy is best explained if the Australian plate contains two component plates. Thus, the traditionally defined Indo-Australian plate consists of three component plates and multiple diffuse plate boundaries. The pattern of present deformation indicates that the boundaries between the three component plates are two unconnected zones accommodating divergence and a larger zone, which we interpret as three diffuse convergent plate boundaries and a diffuse triple junction.**

The plate tectonic idealization of rigid plates and narrow plate boundaries is inconsistent with seismicity and data recording the motion of the Indo-Australian plate (Fig. 1A). The first indications of an inconsistency of plate motion data with a single rigid Indo-Australian plate were the difficulties in simultaneously fitting data along the three mid-ocean ridge (MOR) systems that meet at the Rodrigues triple junction (RTJ): (i) the Southwest Indian Ridge (SWIR), (ii) the Southeast Indian Ridge (SEIR), and (iii) the Central Indian Ridge (CIR) and its northwestern continuation, the Carlsberg Ridge (*1–3*). Moreover, many earthquakes of magnitude 6 or 7 have occurred this century near the Ninetyeast Ridge (90ER) and give a rate of seismic moment release comparable to that along the San Andreas fault in California (*4*). These results suggest a plate motion model in which the Indo-Australian plate is treated as two distinct plates separated by a possibly wide boundary that mainly follows the 90ER and continues southwest from the southern termination of the 90ER to intersect the SEIR near 80°E (*1*), where anomalous off-ridge, normal-faulting earthquakes occur (*5*). This two-plate model fit the Indian Ocean plate motion data significantly better than a single-plate model, but the data were still fit much worse than along other plate boundaries (*1*).

That anomalous off-ridge earthquakes occur near the CIR between about the equator and 10°S (*6*) suggests an alternative model in which the Indo-Australian plate comprises two plates and an intervening east-west (E-W)–striking near-equatorial diffuse boundary (*7*) [or, strictly speaking, two disjoint diffuse boundaries that can be joined by an E-W–striking great circle (*8*)] (Fig. 1B). Plate motion data fit this model significantly better than they fit a model with a north-south (N-S)–striking boundary (*3, 7–12*). This model has been used to predict the average sense, orientation, and magnitude of the integral of deformation or deformation rate across the equatorial diffuse boundary since 3 million years ago (Ma) (*8*) and since 11 Ma (*12*). The main predictions are that the Indian plate is diverging from the Australian plate west of the pole of rotation (5°S, 74°E) and is converging with the Australian plate east of the pole of rotation. Hence, approximately N-S stretching (*13*) is predicted across the deformation zone west of the pole of rotation, as is independently observed from earthquake mechanisms, and approximately N-S shortening is predicted across the deformation zone east of the pole of rotation, as is observed across the Central Indian Basin from ~77° to ~86°E from earthquake mechanisms (*14*) and E-W–striking thrust faults observed along seismic reflection profiles (*15–17*). North-south shortening in the Central Indian Basin is also indicated by the presence of E-W–striking undulations in topography having peak-to-trough amplitudes of ~1 km and wavelengths of 100 to 300 km (*16, 17*). These undulations are associated with 30- to 80-milliGalileo (1 mgal = $10^{-5}$ m $s^{-2}$) peak-to-trough free-air gravity anomalies (*16, 18*), which occur east of about 74°E, that is, from a little east of the Chagos trough to ~86°E, where there is a fracture zone with an apparently large offset (*19*) (Fig. 2).

Although the predictions agree with the deformation observed west of ~86°E in the

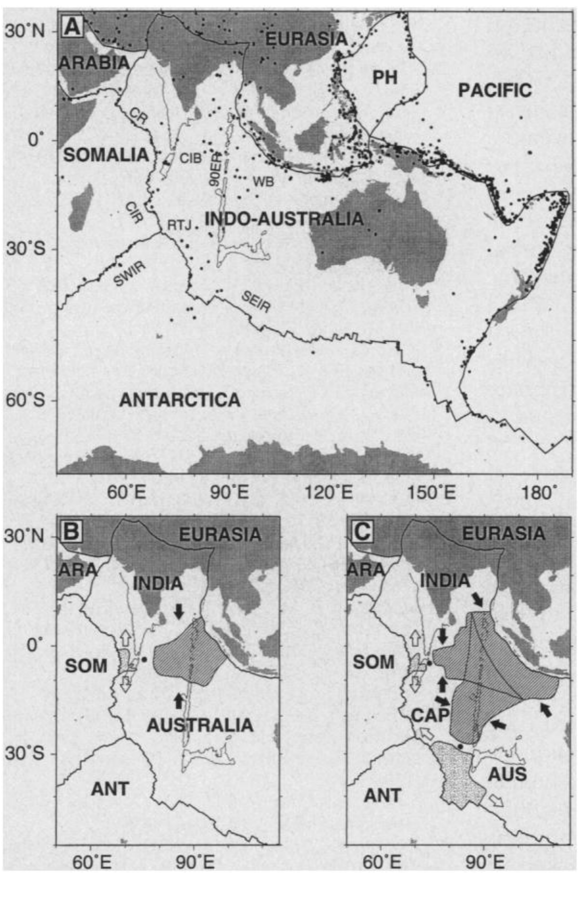


**Fig. 1.** (**A**) Traditional Indo-Australian plate boundaries with locations of earthquakes of magnitude $m_b$ > 5.5 shown by small solid circles. RTJ: Rodrigues triple junction; CR: Carlsberg Ridge; CIR: Central Indian Ridge; SWIR: Southwest Indian Ridge; SEIR: Southeast Indian Ridge; 90ER: Ninetyeast Ridge; CIB: Central Indian Basin; WB: Wharton Basin; and PH: Philippine Sea plate. (**B**) Plate boundary as proposed in (*8*). (**C**) New plate geometry proposed here. CAP: newly recognized Capricorn plate; AUS: redefined Australian plate. Stipples denote diffuse boundaries accommodating horizontal divergence, whereas hatched areas denote diffuse boundaries accommodating horizontal convergence.

J.-Y. Royer is with Géosciences Azur, BP 48, 06235, Villefranche sur mer Cedex, France. R. G. Gordon is with the Department of Geology and Geophysics, MS 126, Rice University, Houston, TX 77005, USA.

Central Indian Basin, they are inconsistent with the deformation observed elsewhere in the diffuse plate boundary and in the supposedly rigid Australian plate. In particular, the model fails to explain the following: (i) why there is NW-SE stretching adjacent to the SEIR near 80°E (*5*), (ii) why the direction of shortening rotates from N-S west of ~86°E to NW-SE east of ~86°, (iii) why NW-SE shortening continues so far south along and southwest across the 90ER, (iv) why there are NE-SW–trending undulations in the gravity field in the Wharton Basin, which presumably indicate NW-SE shortening (*20*, *21*), and (v) why extinct fracture zones in the Wharton Basin are reactivated by N-S left-lateral strike-slip motion (*22*). Here we propose a revised plate geometry (Fig. 1C) and set of angular velocities that are consistent with these observations.

**Plate reconstructions**. We investigate these problems through a detailed analysis of the location of the old end of anomaly 5, which is observed over 11-million-year-old sea floor flanking the SEIR and SWIR. We build on earlier studies of anomaly 5 flanking the CIR (*12*), SWIR, and SEIR (*3*, *23*). We estimate the location of a crossing of anomaly 5 flanking the SEIR or SWIR on many profiles from digital data that were previously unavailable to us (*24*, *25*) (Fig. 3, A and B).

We first tested the consistency with closure of the motions since chron 5 (11 Ma) of the three plates that meet at the RTJ assuming the plate geometry of Fig. 1B (*26*, *27*). The resulting value of the statistic $\Delta r$ is 39.9 (*26*), which has a probability of occurring by chance of 1 part in $10^8$ if the three plates are rigid (*28*).

There is little evidence for deformation of the Antarctic plate, except for a few clustered off-ridge earthquakes between the Kerguelen Plateau and the SEIR. These earthquakes, which have a modest moment release about 1/16 of that of off-ridge events located nearby on the Australian side of the SEIR, can be attributed to the release of thermal and bending stresses associated with a residual depth anomaly between the Kerguelen Plateau and the SEIR (*5*).

We calculated in the Somalian reference frame the rotation needed to close the gap in magnetic-anomaly crossings if the gap is due to a rotation between hypothetical distinct parts of Somalia separated by a boundary intersecting the RTJ, which gives a rotation of 0.52° ± 0.27° (*29*) about a pole located at 29.8°S, 86.0°E. The sense of the rotation going forward in time is not divergence but convergence, if the hypothetical boundary follows the East Africa Rift Valley. Although we cannot exclude the possibility of deformation of Somalia, the hypothesis that such deformation is causing the observed misfit is excludable.

This exclusion leads to the hypothesis of deformation of the Australian plate, for which there is independent evidence, in particular the SSW-striking zone of NW-SE shortening that crosses the 90ER and the zone of NW-SE stretching next to the SEIR (Fig. 2). The calculated rotation between hypothetical NW and SE Australian plates with a boundary that intersects the RTJ is 0.52° ± 0.27° about a pole at 25.8°S, 90.0°E. The sense of rotation indicates NW-SE convergence north and NNE of the pole and NW-SE divergence SW of the pole.

To carry the analysis further, we segregated the magnetic-anomaly and fracture-zone crossings flanking the SEIR into three groups: (i) crossings NW of the portion of the SEIR adjacent to the zone of off-ridge earthquakes, which are assumed to record motion between the Antarctic plate and the newly recognized Capricorn plate (Fig. 1C), (ii) crossings flanking the portion of the SEIR adjacent to the zone of off-ridge earthquakes, and (iii) crossings flanking the portion of the SEIR southeast of the zone of

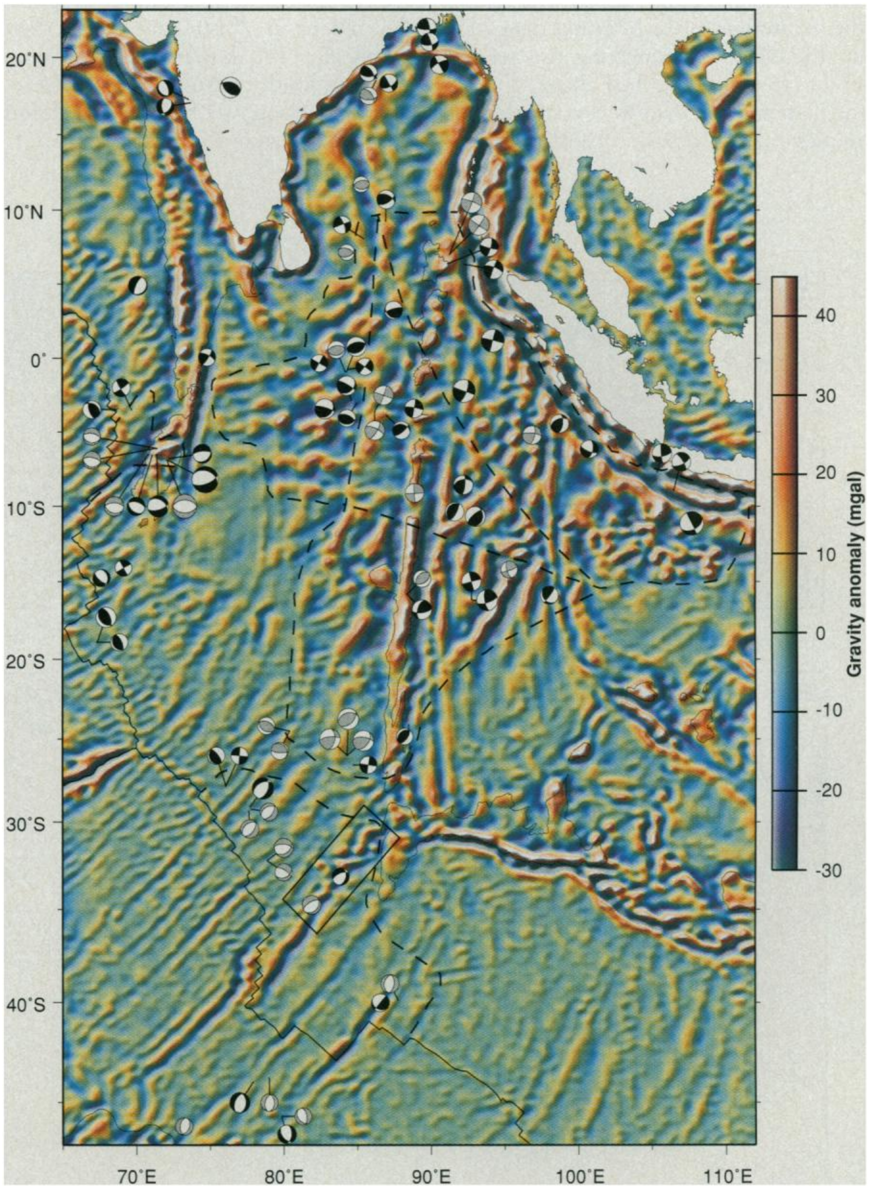


**Fig. 2.** Tectonic map of the Indian Ocean showing focal mechanisms for earthquakes with moments > 3 × $10^{23}$ dyne•cm [black-filled mechanisms are Harvard CMT solutions; gray-filled mechanisms are from (*5*, *46*)] and a bandpass filtered (150- to 300-km wavelength) version of the gravity grid of (*19*). The dashed lines show the edges of the tectonic boundaries discussed in this paper. An en échelon array of ridges, which lie southwest of the 90ER (inside the rectangle), may be volcanic in origin and may have accommodated some of the divergence between the Capricorn and Australian plates (Fig. 1C).

off-ridge earthquakes, which are assumed to record motion between the Antarctic plate and a redefined Australian plate (Fig. 1C). This plate geometry is consistent with closure of the Antarctic-Somalian-Capricorn plate circuit (Fig. 4, B and C), with $\Delta r$ = 5.0, which has a probability of being exceeded by chance of 17% if the three plates are rigid (*30*). When the resulting Capricorn-Antarctic rotation is applied to the redefined Australian plate, there is a gap of ~40 km in magnetic anomaly crossings south of Australia (Fig. 4A). Thus, the nonclosure about the RTJ must be caused by deformation that intersects the SEIR east of about 75°E.

We obtained a direct test of the rigidity of the Australian plate by using data only along the SEIR and omitting the second group of crossings described above. The fit to the plate motion data were compared for two cases: (i) the first and third groups of crossings were assumed to record the motion of a single Australian plate relative to the Antarctic plate, and (ii) the first group was assumed to record the motion of the Capricorn plate relative to the Antarctic plate, and the third group, the motion of the east Australian plate relative to the Antarctic plate. The comparison gave $\Delta r$ = 21.0, which has a probability of occurring by chance of $10^{-4}$ if there is a single rigid Australian plate (Fig. 1B) (*31*). Thus, we conclude that the motion between the Capricorn and Australian plates is also statistically significant from only data along the SEIR (*32*). When the Capricorn-Antarctic rotation estimated only from data along the Capricorn-Antarctic boundary is applied to the redefined Australian plate, there is a gap of ~140 km in magnetic-anomaly crossings south of Australia (Fig. 4A).

**Comparison with present deformation.** If one assumes the existence of distinct Capricorn and Australian plates, their pole of relative rotation can be estimated from the present pattern of deformation. The pole must lie to the NE of the zone of NW-SE stretching and to the SW of the zone of NW-SE shortening, which tightly limits its position to near that shown in Fig. 1C; positions slightly to the NW or ESE of where it is shown in Fig. 1C are also consistent with the pattern of deformation.

The plate reconstructions indicate a rotation of 0.78 ± 0.30° about 29.1°S, 90.3°E (Fig. 5) (*33*). The confidence region of the pole from plate reconstructions includes the region inferred from the deformation pattern, indicating the consistency of the plate reconstructions with the observed current pattern of deformation. The confidence limits from plate reconstructions is large, however.

The plate reconstructions indicate that

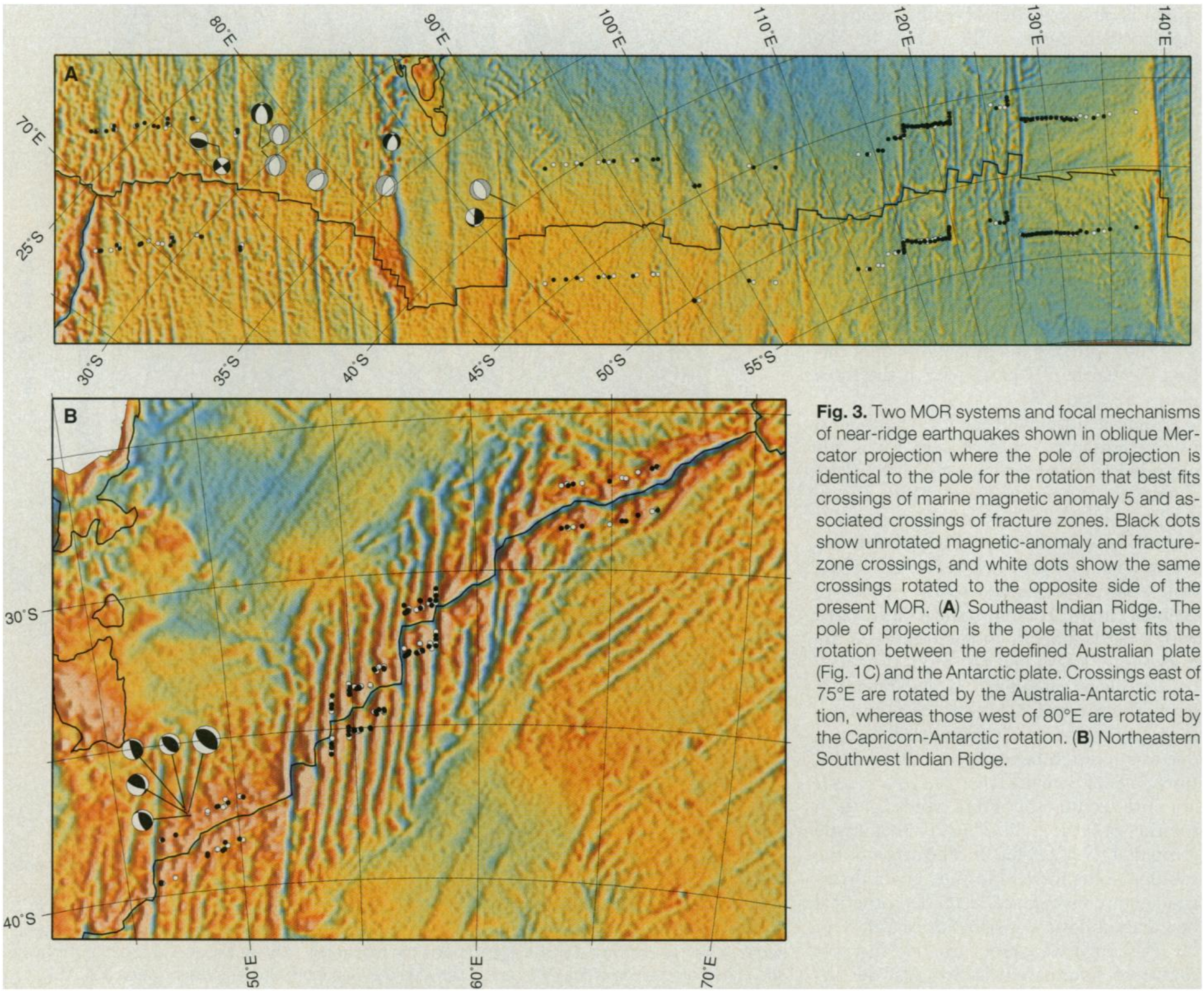


**Fig. 3.** Two MOR systems and focal mechanisms of near-ridge earthquakes shown in oblique Mercator projection where the pole of projection is identical to the pole for the rotation that best fits crossings of marine magnetic anomaly 5 and associated crossings of fracture zones. Black dots show unrotated magnetic-anomaly and fracture-zone crossings, and white dots show the same crossings rotated to the opposite side of the present MOR. (**A**) Southeast Indian Ridge. The pole of projection is the pole that best fits the rotation between the redefined Australian plate (Fig. 1C) and the Antarctic plate. Crossings east of 75°E are rotated by the Australia-Antarctic rotation, whereas those west of 80°E are rotated by the Capricorn-Antarctic rotation. (**B**) Northeastern Southwest Indian Ridge.

since 11 Ma, a point now at 17°S, 105°E on the Australian plate has moved 27.0 km approximately along N45°W relative to an arbitrarily fixed Capricorn plate. The plate reconstructions indicate convergence of 23 ± 26 km since 11 Ma between the Capricorn plate (10.3°S, 83.5°E) and the Australian plate (17°S, 105°E), corresponding to a rate of 2.1 ± 2.4 mm/year, which is not only much slower than the global median rate of convergence at trenches (~70 mm/year) but is also less than the slowest (~20 mm/year) rate of trench convergence (*34*). This convergence, although slow, may have produced large earthquakes and large-scale folding of the lithosphere, as suggested by the undulations in gravity, which strike NE and occur both east and west of 90ER (Fig. 2). The reconstructions also indicate divergence of 13 ± 24 km since 11 Ma between the Capricorn plate (26°S, 74°E) and the Australian plate (41°S, 90°E), corresponding to a rate of 1.2 ± 2.2 mm/year, which is not only much slower than the global median rate of spreading at MORs (~40 mm/year) but is also less than the slowest (~10 mm/year) rate of sea-floor spreading (*35*).

The plate reconstructions therefore suggest a unified kinematic explanation for the existence of the southwestern zone of NW-SE stretching, the existence of the northeastern zone of NW-SE shortening, the cause of the change in direction of shortening from N-S west of ~86°E in the equatorial zone of deformation to NW-SE east of ~86° in the equatorial zone, and the existence of NW-SE shortening south and southwest of the 90ER. These changes are herein viewed as a consequence of the relative rotations of the Indian, Capricorn, and Australian plates. The pole of rotation between the Indian and Capricorn plates has small confidence limits and lies in the narrow region between the western zone of N-S stretching and the eastern zone of N-S shortening (Fig. 5). The stretching portions of both diffuse plate boundaries intersect a MOR, and the stretching direction in both cases is nearly parallel with the overall strike of the combined MOR and transform fault geometry. The India-Capricorn and Capricorn-Australia zones of shortening merge and are terminated by an overriding plate at a subduction zone. These characteristics, having a pole of rotation lying between a zone of stretching next to a MOR system and a zone of shortening next

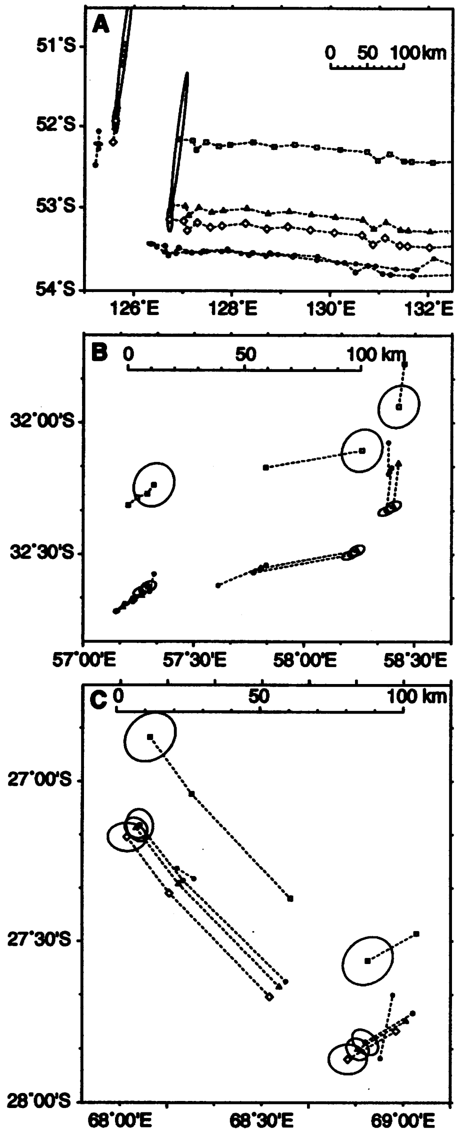


**Fig. 4.** (**A**) Crossings flanking the Southeast Indian Ridge south of Australia (Fig. 3A); the Antarctic plate (solid symbols) was held fixed, and data from the redefined Australian plate (open symbols) were rotated about a pole describing their relative motion since chron 5 (11 Ma). Four different rotations are compared: (open circles) the Australia-Antarctic best-fitting rotation; (diamonds) the Capricorn-Antarctic rotation predicted from summing the best-fitting Capricorn-Somalia and Somalia-Antarctic rotations; (triangles) the Capricorn-Antarctic rotation predicted by the Capricorn-Somalia-Antarctic three-plate solution consistent with closure; and (squares) the best-fitting Capricorn-Antarctic rotation. Ellipses show 95% uncertainty regions of representative reconstructed points. Kilometer scale is correct at 53°S. (**B**) Crossings flanking part of the northeastern Southwest Indian Ridge (Fig. 3B); the Antarctic plate (solid symbols) was held fixed, and data from the Somalian plate (open symbols) were rotated about a pole describing their relative motion since chron 5 (11 Ma). Three different rotations are compared: (open circles) the Somalia-Antarctic best-fitting rotation; (squares) the Somalia-Antarctic rotation predicted from closure, as if the Capricorn and Australian plates formed a single plate (that is, summing the Somalia-Capricorn and Australia-Antarctic rotations); and (triangles) the Somalia-Antarctic rotation predicted by the Capricorn-Somalia-Antarctic three-plate solution. Ellipses show 95% uncertainty regions of representative reconstructed points. Kilometer scale is correct at 32°S. (**C**) Crossings flanking part of the northwestern Southeast Indian Ridge (Fig. 3A); the Antarctic plate (solid symbols) was held fixed, and data from the Capricorn plate (open symbols) were rotated about a pole describing their relative motion since chron 5 (11 Ma). Four different rotations are compared: (open circles) the Capricorn-Antarctic best-fitting rotation; (diamonds) the Capricorn-Antarctic rotation predicted from summing the best-fitting Capricorn-Somalia and Somalia-Antarctic rotations; (triangles) the Capricorn-Antarctic rotation predicted by the Capricorn-Somalia-Antarctic three-plate solution; and (squares) the Australia-Antarctic best-fitting rotation. Ellipses show 95% uncertainty regions of representative reconstructed points. Kilometer scale is correct at 28°S.

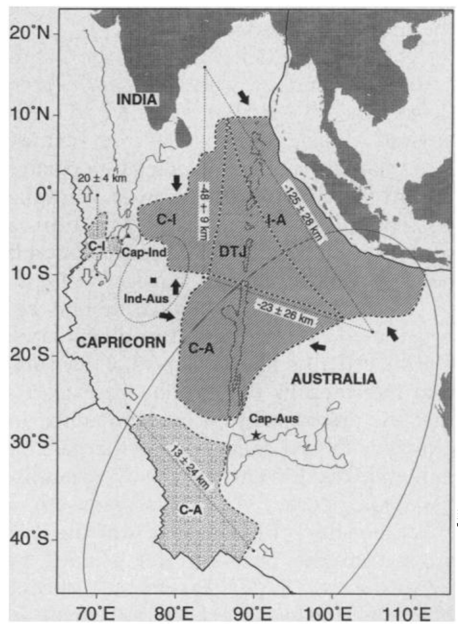


**Fig. 5.** Wide deformation zones (outlined by dashed lines) between the Indian, Capricorn, and Australian plates. Zones accommodating convergence are hatched; zones accommodating divergence are stippled. The three component plates, the Indian plate, Capricorn plate, and Australian plate, are labeled; "C-I" is the Capricorn-India boundary; "C-A," the Capricorn-Australia boundary; "I-A," the India-Australia boundary; and "DTJ," the diffuse triple junction where the three boundaries meet. Poles of relative rotation and associated 95% confidence limits determined from plate reconstruction data are also shown. The confidence regions for the Capricorn-India and Capricorn-Australia poles of rotation determined from plate reconstruction data include the poles of rotation inferred from present deformation (solid circles in Fig. 1C). Amount of motion (and one-dimensional 95% confidence limits) since 11 Ma are given along some baselines across the diffuse boundaries; negative values indicate convergence and positive values indicate divergence.

to a subducting slab, are shared with the diffuse plate boundary between the North and South American plates in the equatorial Atlantic (*36*). None of these deformation zones seem related to preexisting zones of weakness, suggesting that they are simply located where the deviatoric stresses due to externally imposed tectonic forces were the greatest.

Averaged over the past 11 million years, the rate of rotation between the Indian and Capricorn plates is $0.24 \pm 0.02°$ per million years, whereas that between the Capricorn and Australian plates is $0.07 \pm 0.03°$ per million years. That the rotation rate about the Capricorn-Australian pole is slower than that about the India-Capricorn pole helps to explain why the confidence region for the former is larger than that for the latter, and why it has taken longer to resolve the motion between the Capricorn and Australian plates than that between the Indian and Capricorn plates.

The average motion between the Capricorn and Antarctic plates may have been slower since 3 Ma than since 11 Ma. An obvious change in strike of the fracture zones flanking the SEIR indicates a change toward more eastward motion of Australia relative to Antarctica at ~4 Ma; thus, a recent slowing or other change in motion is possible and may explain why DeMets *et al.* (*8, 9*) were unable to resolve motion between the Capricorn and Australian plates. On the other hand, the pattern of deformation indicated by the earthquakes suggests that the present motion remains similar in direction to the average over the past 11 million years. Given that the average misfits in rate of only ~4 to 5 mm/year south of Australia and 1 to 2 mm/year near the RTJ are within the uncertainties assumed by DeMets *et al.* (*8, 37*), the motion since 3 Ma may simply have been too small to resolve.

Figure 5 shows the location of the two zones of horizontal stretching and the composite zone of horizontal shortening. We infer that the zone of shortening consists of four regions: (i) that between the Indian and Capricorn plates, (ii) that between the Australian and Capricorn plates, (iii) that arguably between the Indian and Australian plates (*38*), and (iv) a triangular-shaped triple junction where these three zones meet. The shortening direction in each portion of the composite zone of shortening agrees with this interpretation. There is N-S shortening in most of the India-Capricorn zone with NW-SE shortening in what we interpret as the northernmost portion of this zone. There is NW-SE shortening in the Capricorn-Australian zone. The pattern is more variable in the wide zone between the Indian and Australian plates but is mainly NW-SE shortening.

It is believed that mountain ranges can occur only in the continents because of the differences in rheology and buoyancy between continental and oceanic crust and lithosphere (*39*). We think that these beliefs require modification. Horizontal shortening and vertical thickening must be occurring where the Indian, Capricorn, and Australian plates converge. Insofar as the ~100- to 300-km wavelength undulations in gravity reflect undulations in the topography, this region would probably be described as a fold and thrust mountain range, albeit of modest amplitude, if it existed on a continent. According to long-standing concepts of plate tectonics, convergence of oceanic lithosphere is accommodated by the thrusting of one oceanic tectonic plate beneath another. That a fold and thrust mountain range may instead have formed indicates that the contrasts in strength and buoyancy profiles of oceanic and continental lithosphere is an incomplete explanation for the difference in their response to convergence and suggests that convergence rate may also be an important factor.

The earthquake mechanisms indicate that the divergence between the Capricorn and Australian plates along the SEIR is mainly taken up by normal faulting, with the stretching direction being nearly parallel to the strike of the SEIR. The $13 \pm 24$ km of divergence in 11 million years is apparently accommodated by widely distributed thinning of the crust and lithosphere by normal faulting and may be partly accommodated by the filling of cracks in the lithosphere by magma. Between about 29°S, 87°E and 36°S, 80°E is an en échelon set of NE- to ENE-striking ridges that are individually oblique to the fracture zone topography (region enclosed in a rectangle on Fig. 2). We are unaware of any sampling of these ridges, almost none of which appear on the GEBCO bathymetric charts (*40*), but their images on the satellite-derived gravity grid suggest that they are volcanic edifices. Two normal-faulting earthquakes of magnitude ($m_b$) 5.9 and 5.4 have occurred along this en échelon line of ridges (Fig. 2). We speculate that at least some of the divergence between the Capricorn and Australian plates is accommodated by the formation of these volcanic ridges.

This behavior differs from that in the western portion of the zone of N-S stretching between the Indian and Capricorn plates, where the deformation appears to be taken up mainly by right-lateral strike-slip faulting along NE-striking fracture zones. The pattern of deformation there implies that the crustal or lithospheric blocks between the fracture zones must be rotating counterclockwise as part of the deformation needed to accommodate N-S divergence (*8, 12*).

**Implications for the plate tectonic approximation.** In our view, the central tenet of plate tectonics is that plate interiors can be usefully approximated as being rigid. In that sense, our model is consistent with plate tectonics as long as the Indian, Capricorn, and Australian components, and not the Indo-Australian composite, are each considered to be a plate. The key assumption of traditional plate tectonics (*41*) that requires modification is that all oceanic plate boundaries are narrow (*7*). Because the rates of divergence and convergence accommodated across these diffuse plate boundaries are slow relative to those across typical narrow boundaries and because the component plates are mechanically coupled more strongly than are plates divided by typical narrow boundaries, it makes sense to regard the Indo-Australian "plate" as a higher level plate tectonic unit, which we refer to as a composite plate. Other composite plates under this scheme of classification include the American plate, with North and South American plate components, and the African plate, with Nubian and Somalian plate components.

Because our model requires more plates, more adjustable parameters are needed to describe the motion of the plates, which is less elegant but more realistic than traditional plate tectonics. Moreover, plate tectonics across diffuse boundaries is less predictive than plate tectonics across narrow boundaries (*42*) .

The area of deformation related to the composite plate boundary, which exceeds the size of several plates, may be even larger than we show in Fig. 5, which would further reduce the area of rigid or nearly rigid plates. Many earthquakes with magnitudes > 5.5 occur outside the area that we indicate as being a plate boundary zone. Prominent examples include the magnitude 6.3 thrust earthquake in the interior of the Indian subcontinent (29 September 1993), six events in the northern Bay of Bengal, the northeasternmost three of which appear to align on what may be a major strike-slip fault, and many earthquakes within the Australian continent.

The consistency of the plate reconstructions suggests little deformation within at least some portions of the Indian, Somalian, Capricorn, and Australian plates, however. First, the consistency of the Capricorn, Somalian, and Antarctic plates with plate circuit closure since chron 5 suggests that little deformation occurs within their interiors, or at least those portions of the interiors near the MORs meeting at the RTJ. Second, the consistency of the Indian, Somalian, and Arabian plates with plate circuit closure since anomaly 2A similarly suggests that little deformation occurs within their interiors, or at least those portions of the interiors near the Carlsberg Ridge, Sheba Ridge, and Owen fracture zone (*8*). Third, the fit to marine magnetic-anomaly and fracture-zone data from the Indian plate with that from the Somalian plate along the Carlsberg Ridge north of ~7°S leaves little room for deformation of the portion of the Indian plate near the Carlsberg Ridge (*12*). Fourth, the fit of marine magnetic-anomaly and fracture-zone data between the Capricorn and Somalian plates along the CIR south of ~11°S leaves little room for deformation of the Capricorn plate near the CIR (*12*). Fifth, geodetic data from very long baseline interferometry (VLBI) places upper limits on deformation within a portion of the Australian plate. A conservative error budget for the geodetic data indicates that the geodesic distance between the telescope sites at Tidbinbilla and Hobart, the two sites on Australia, is decreasing at an insignificant rate of 1.3 ± 3.8 mm/year (95% confidence limits) across a distance of 830 km (*43*). This value places an upper bound of 5.1 mm/year on convergence between the two sites.

Perhaps a more useful but less rigorous limit on deformation comes from examination of the total divergence and convergence rates across the diffuse plate boundaries. The high level of near-ridge seismicity and consistency of the focal mechanisms for the zone of stretching flanking the SEIR is unusual (*5*). The zones of nearly ridge-parallel stretching flanking the CIR and SEIR (Figs. 2 and 5) are alone in the world's oceans in having significant seismicity showing a consistent sense of distributed stretching. The inferred average divergence rate between the Capricorn and Australian plates along the SEIR is 1.3 ± 2.2 mm/year (Fig. 5). We speculate that any near-ridge deformation elsewhere with less seismicity is diverging at a rate lower than the implied upper bound of 3.5 mm/year across the boundary between the Capricorn and Australian plates. A similar argument applies to the region of shortening between the Capricorn and Australian plates. In the northeasternmost portion of the Capricorn-Australia convergent plate boundary, the convergence rate is 2.4 ± 2.4 mm/year and decreases to the southeast to 0.5 ± 1.9 mm/year near 25°S, 85°E. We speculate that any diffuse oceanic convergence elsewhere with less seismicity is occurring at a rate lower than the upper bound of 4.8 mm/year. Given that the motion across these zones of deformation marked by unusual seismicity is so slow, it seems likely that intraplate motion due to the background level of intraplate deformation in the oceans is even lower, a few millimeters per year, unless the record of seismicity for a given region is unrepresentative of the longer term deformation. The upper bound on the integral of intraplate continental deformation rate from geodetic data from VLBI, which is 2 mm/year for the nine best-observed sites in the North American and western European interiors (*43*), gives a similar small upper bound on intraplate motion.

## REFERENCES AND NOTES


1. J. B. Minster and T. H. Jordan, *J. Geophys. Res.* **83**, 5331 (1978); S. Stein and R. G. Gordon, *Earth Planet. Sci. Lett.* **69**, 401 (1984).
2. R. G. Gordon, S. Stein, C. DeMets, D. F. Argus, *Geophys. Res. Lett.* **14**, 587 (1987).
3. J.-Y. Royer and T. Chang, *J. Geophys. Res.* **96**, 11779 (1991).
4. S. Stein and E. A. Okal, *ibid.* **83**, 2233 (1978).
5. E. A. Bergman, J. L. Nabelek, S. C. Solomon, *ibid.* **89**, 2425 (1984).
6. S. Stein, *Geophys. J. R. Astron. Soc.* **55**, 577 (1978); D. A. Wiens, *Earth Planet. Sci. Lett.* **76**, 350 (1986).
7. D. A. Wiens *et al.*, *Geophys. Res. Lett.* **12**, 429 (1985).
8. C. DeMets, R. G. Gordon, P. Vogt, *Geophys. J. Int.* **119**, 893 (1994).
9. C. DeMets, R. G. Gordon, D. F. Argus, *J. Geophys. Res.* **93**, 11877 (1988).
10. R. G. Gordon and C. DeMets, *ibid.* **94**, 5560 (1989).
11. ——— and D. F. Argus, *Tectonics* **9**, 409 (1990).
12. J.-Y. Royer, R. G. Gordon, C. DeMets, P. Vogt, *Geophys. J. Int.* **129**, 41 (1997).
13. Herein, a direction of stretching refers to the orientation of the maximum principal axis of stretching. Similarly, a direction of shortening refers to the orientation of the minimum principal axis of stretching, or equivalently, the maximum principal axis of shortening.
14. E. A. Bergman and S. C. Solomon, *Phys. Earth Planet. Inter.* **40**, 1 (1985).
15. J. R. Curray and D. G. Moore, *Geol. Soc. Am. Bull.* **82**, 563 (1971); S. Eittreim and J. Ewing, *J. Geophys. Res.* **77**, 6413 (1972); D. G. Moore, J. R. Curray, R. W. Raitt, F. J. Emmel, *Initial Rep. Deep Sea Drill. Proj.* **22**, 403 (1974); Y. P. Neprochnov, O. V. Levchenko, L. R. Merklin, V. V. Sedov, *Tectonophysics* **156**, 89 (1988); J. M. Bull, *ibid.* **184**, 213 (1990); J. M. Bull and R. A. Scrutton, *Nature* **344**, 855 (1990); N. Chamot-Rooke, F. Jestin, B. de Voogd, Phèdre Working Group, *Geology* **21**, 1043 (1993).
16. J. K. Weissel, R. N. Anderson, C. A. Geller, *Nature* **287**, 284 (1980).
17. C. A. Geller, J. K. Weissel, R. N. Anderson, *J. Geophys. Res.* **88**, 1018 (1983).
18. D. C. McAdoo and D. T. Sandwell, *ibid.* **90**, 8563 (1985).
19. D. T. Sandwell and W. H. F. Smith, *ibid.* **102**, 10039 (1997).
20. D. E. Petroy and D. A. Wiens, *ibid.* **94**, 12301 (1989).
21. C. A. Stein, S. Cloetingh, R. Wortel, *Geophys. Res. Lett.* **16**, 823 (1989).
22. H. Hebert *et al.*, *Eos* **46**, F684 (1996).
23. J.-Y. Royer and R. Schlich, *J. Geophys. Res.* **93**, 13524 (1988).
24. The location of each crossing of the old end of anomaly 5 is identified along a ship-board magnetic profile or aeromagnetic profile, which come from many sources. To avoid the loss of resolution inherent in digitizing analog records, especially from published figures, we used digital data whenever available. The magnetic-anomaly crossings flanking the CIR are taken from (*12*), except for the southernmost crossing of anomaly 5 on the Indo-Australian side of the MOR, which we now believe lies over sea floor created at the SEIR (Fig. 3A). The magnetic-anomaly crossings flanking the SWIR (Fig. 3B) have been redetermined and incorporate many unavailable to (*3*). Crossings west of 46°E have been excluded to avoid the portion of the SWIR recording motion between the Antarctic and Nubian plates and the deforming zone assumed to exist between the Nubian and Somalian plates (*44*). Thus, the new set of crossings are expected to record motion between the Antarctic and Somalian plates. We have added new crossings and reidentified many other crossings of anomaly 5 flanking the SEIR. There is thus little overlap with Royer and Chang's (*3*) set of magnetic-anomaly crossings flanking the SEIR. As in (*3*), we exclude data east of ~140°E to avoid the southeast corner of the Australian plate, which has been hypothesized to be deforming in response to convergence with the Pacific plate (*9*, *45*).
25. The location of each crossing of a fracture zone is determined from satellite-derived gravity data. Along the CIR, the locations are crossings along individual processed profiles and are identical to those used by (*12*). Along the other two MOR systems, the crossings are interpreted from a gridded gravity map (*19*). The center of the fracture zone is assumed to lie at the center of the gravity trough for all fracture zones flanking the SWIR and CIR, which are spreading slowly and presumably resemble the morphology of the better studied fracture zones along the slowly spreading Mid-Atlantic Ridge. The signature of fracture zones flanking the SEIR is more complex. Royer and Sandwell (*45*) estimated the locations of fracture-zone crossings assuming that the maximum slope in the calculated gravity (that is, roughly midway between an adjacent gravity peak and trough) lies over the center of the fracture zone, as is expected at a fast-spreading MOR such as the East Pacific Rise. The gravity grid from declassified Geosat data (*19*) indicates that the signature of fracture zones flanking the SEIR varies considerably from fracture zone to fracture zone. Some zones appear highly antisymmetric with respect to the SEIR with a fracture-zone trough on one side of the MOR correlating with a fracture-zone ridge on the other side; this indicates that the maximum slope between fracture-zone ridge and trough on one side of the MOR should be correlated with that on the other. Other fracture zones, however, resemble those along slowly spreading MORs, with a fracture-zone trough on one side of the MOR correlating with a trough on the other side. We selected for analysis three fracture zones south of Australia resembling those on slowly spreading ridges (Fig. 3A). Also needed were sets of fracture-zone crossings along the westernmost SEIR, which lacks clear, straight fracture zones that are continuous between anomaly 5 and the SEIR. For this region, we correlated the midpoint between fracture-zone ridge and trough on one side of the MOR with the midpoint on the other side of the MOR for three fracture zones that clearly offset anomaly 5 by about 30, 50, and 70 km from the westernmost to the easternmost fracture zone, respectively (Fig. 3A). We investigated the self-consistency of the interpretation of fracture-zone crossings and the resulting reconstructions by examining the distance between the nearest magnetic-anomaly crossing to a given fracture zone and the distance of the same crossing when reconstructed across the MOR from what was interpreted as the correlative feature. The interpreted crossings are consistent with our best-fitting rotations. The self-consistency was further investigated by matching up conjugate wandering offsets lying just NW of a fracture zone that intersects the SEIR near 32°S, 77°E (Fig. 3A). The three offsets match up within ~10 km, consistent with our interpretation.
26. The best-fitting rotations and their uncertainties were found with the use of the methods of Chang [(*3*); T. Chang, *J. Am. Stat. Assoc.* **83**, 1178 (1988)], which use the Hellinger fitting criterion [S. J. Hellinger, *J. Geophys. Res.* **86**, 9312 (1981)]. These methods allow us to estimate the dispersion of the data or subsets of the data. They produce a statistic $r$, which is expected to be chi-square distributed with $\nu$ degrees of freedom; $r$ is the sum-squared normalized misfit of the magnetic-anomaly and fracture-zone crossings to the best-fitting model. The degrees of freedom $\nu$ equals $N - 3m - 2n$, where $N$ is the number of magnetic-anomaly and fracture-zone

crossings, $m$ is the number of independent rotations to be estimated, and $n$ is the number of data segments used. A data segment can consist of three or more fracture-zone crossings that sample the same fracture zone; at least one crossing must come from each side of a MOR. A data segment can also consist of three or more magnetic-anomaly crossings that sample the same MOR segment between fracture zones or a subset of a ridge segment if the segment is long; at least one crossing must come from each side of the present MOR. In the inversion procedure, a great circle is fit to each data segment and requires two adjustable parameters. The precision parameter $\hat{\kappa}$ is the ratio of $\nu$ to $r$. If a subset of crossings are input to the rotation parameter-fitting program, each with a nominal error of $\sigma_{nom}$, then the precision parameter can be used to estimate the standard deviation of the crossings as $\sigma_{nom}/\hat{\kappa}^{1/2}$. We typically use $\sigma_{nom}$ = 10 km. We use the estimated standard deviations as an aid in formulating error budgets for the data. To test for the consistency with plate-circuit closure of plate motion data along three plate boundaries meeting at a triple junction, we typically use the following chi-square test. We estimate a statistic $\Delta r$, which is the difference in $r$ between a model in which closure is enforced about the three-plate circuit and a model in which closure is unenforced. In the latter case, $r = r_1 + r_2 + r_3$, where each $r_i$ is the $r$ for a best-fitting rotation, as described above. Three is the number of independent rotations estimated (that is, $m$). Thus, $r$ is expected to be chi-square distributed with three degrees of freedom.

27. Uncertainties in the data were mainly assigned from preliminary estimates of the standard deviation of subsets of data. Error assignments for crossings along the CIR are identical to those assigned by (*12*). In brief, all fracture-zone crossings along the CIR were assigned errors of 5 km. Magnetic-anomaly crossings along the CIR were divided into four groups, mainly based on when the magnetic profiles were acquired, with the oldest profiles being assigned the largest uncertainties (1$\sigma$ error of 5.2 km), the most recently acquired profiles being assigned the smallest error (1$\sigma$ error of 3.0 km), and the two intermediate groups being assigned errors of 3.2 km and 3.9 km. Magnetic-anomaly crossings along the SWIR were assigned a 1$\sigma$ error of 4 km, whereas fracture-zone crossings along the SWIR were assigned a 1$\sigma$ error of 5 km. The dispersion of the data indicates that the uncertainties should be 30 to 40% smaller, but we are reluctant to shrink the assigned errors further. Along the SEIR, fracture-zone crossings were assigned a 1$\sigma$ error of 6 km. West of ~78°E along the SEIR, where we reexamined the magnetic-anomaly profiles in detail and where the dispersion is low, we assigned a 1$\sigma$ error of 4 km to the magnetic-anomaly crossings. The dispersion of these crossings along the western SEIR indicate that the error should be about three times smaller, but we are reluctant to assign smaller errors based on such a small data set. The 102 magnetic-anomaly crossings along the SEIR east of ~85°E were assigned a 1$\sigma$ error of 5 km, except for 12 crossings from the Eltanin cruises, which were assigned a larger error of 10 km because these profiles were collected in the 1960s, before the advent of satellite navigation, and have highly dispersed crossings of anomaly 5.
28. Inasmuch as the precision parameter $\hat{\kappa}$ for individual plate pairs exceeds 1 for each plate pair (and exceeds 2 in two of the three cases), it seems more likely that we have overestimated rather than underestimated the errors.
29. All uncertainties following "±" signs in this paper are 95% confidence limits.
30. Even if we use the more restrictive $F$-ratio test for closure, which is equivalent to assuming that all errors assigned to the data are overestimated by a uniform multiplicative constant, a value of $F$ of 2.196 is obtained. This value has a 9% probability of occurring by chance if the plates are rigid and is therefore consistent with closure.
31. We make a test analogous to that described in (*26*) when testing if a previously undemonstrated plate boundary intersects a known plate boundary. In this case, $\Delta r$ is the difference between $r$ for a model in which only one plate separates from a second plate along a known plate boundary and $r$ for a model in which two distinct plates separate along the known plate boundary from a third plate. The latter value of $r$ is given by $r_1 + r_2$.
32. If the fracture-zone crossings are omitted from the western SEIR data, the data are still significantly misfit. The value of $\Delta r$ is 14.2 with three degrees of freedom, which has a probability of being exceeded by chance of less than 0.003.
33. The complete covariance matrix for the rotation is $C_{xx} = 2.0735 \times 10^{-6}$, $C_{xy} = 0.1012 \times 10^{-6}$, $C_{xz} = -1.5894 \times 10^{-6}$, $C_{yy} = 5.8913 \times 10^{-6}$, $C_{yz} = -1.8641 \times 10^{-6}$, and $C_{zz} = 4.3707 \times 10^{-6}$ sr, where the $x$, $y$, and $z$ axes parallel (0°N, 0°E), (0°N, 90°E), and 90°N, respectively.
34. C. DeMets, R. G. Gordon, D. F. Argus, S. Stein, *Geophys. J. Int.* **101**, 425 (1990); R. G. Gordon, in *Global Earth Physics: A Handbook of Physical Constants*, T. J. Ahrens, Ed. (AGU Reference Shelf 1, American Geophysical Union, Washington, DC, 1995), pp. 66–87.
35. This low rate of spreading likely occurs in the Red Sea (*44*).
36. D. F. Argus, thesis, Northwestern University (1990); D. F. Argus and R. G. Gordon, unpublished manuscript.
37. DeMets *et al.* (*8*) recently reexamined the consistency of 0- to 3-Ma plate motion data with closure about the RTJ. If they assumed that all the data uncertainties were overestimated by a uniform multiplicative constant, their data are inconsistent with closure at the 0.03% significance level. This result is not completely convincing, however. If they test for closure using the errors assigned to the data, the nonclosure is insignificant. Moreover, the errors they assigned to azimuths of transform faults along the CIR are realistic but inconsistent with those carried over from earlier work along the other two ridge systems. Therefore, further analysis of the 0- to 3-Ma data is required before the case for or against significant nonclosure can be made convincing. In any event, their results place an upper bound on the integral of possible deformation rate around this circuit of ~4 to 7 mm/year, which is large enough to allow deformation as large as we find here.
38. M. J. Tinnon *et al.* [*J. Geophys. Res.* **100**, 24315 (1995)] used earthquake moment tensor data to estimate the pole of rotation between previously defined Indian and Australian plates. Their pole of rotation (10°S, 81°E), although differing insignificantly from what we now interpret as the India-Capricorn pole of rotation, is in even better agreement with the new pole of rotation of India relative to Australia. This is encouraging because many of the earthquakes they analyzed are from what we now interpret as the Capricorn-Australia and India-Australia deforming zones, as well as the triple junction where the three zones of shortening meet.
39. P. Molnar, *Nature* **335**, 131 (1988).
40. R. L. Fisher, M. Z. Jantsch, R. L. Comer, *General Bathymetric Chart of the Oceans (GEBCO)* (Canadian Hydrographic Service, Ottawa, 1982), sheet 5.09.
41. J. T. Wilson, *Nature* **207**, 343 (1965); D. McKenzie and R. L. Parker, *ibid.* **216**, 1276 (1967); W. J. Morgan, *J. Geophys. Res.* **73**, 1959 (1968); X. Le Pichon, *ibid.*, p. 3661.
42. Plate motions predicted across a narrow plate boundary are very specific, consisting of an explicit prediction of the displacement or velocity across or along any point on the narrow plate boundary. Motions predicted across a wide boundary specify only the integral of the deformation or velocity gradient along a path crossing the wide boundary and connecting a point on one rigid plate to a point on another [J. B. Minster and T. H. Jordan, in *Tectonics and Sedimentation Along the California Margin*, J. K. Crouch and S. B. Bachman, Eds. (Pacific Section of the Society of Economic Mineralogists and Paleontologists, Los Angeles, CA, 1984), vol. 38, pp. 1–16].
43. D. F. Argus and R. G. Gordon, *J. Geophys. Res.* **101**, 13555 (1996).
44. D. Chu and R. G. Gordon, in preparation.
45. J.-Y. Royer and D. T. Sandwell, *J. Geophys. Res.* **94**, 13755 (1989).
46. O. V. Levchenko, *Tectonophysics* **170**, 125 (1989).
47. This work was supported by CNRS and Plan National de Télédétection Spatiale, the NSF-CNRS U.S.-France cooperative program (NSF grant INT-9314549), and NSF grant OCE-9596284 (R.G.G.). The figures were drafted using the GMT software [P. Wessel and W. H. F. Smith, *Eos* **372**, 441 (1991)]. Géosciences Azur contribution number 111.

4 February 1997; accepted 13 June 1997